NAWCWPNS TP 8152

DIELECTRIC MODELS IN ADHESION AND EXTRAPOLATIONS OF MOLECULAR MODELING

by

N. E. Iwamoto
Research Department

APRIL 1994

NAVAL AIR WARFARE CENTER WEAPONS DIVISION
CHINA LAKE, CA 93555-6001

Naval Air Warfare Center Weapons Division

FOREWORD

This report documents a theoretical review of adhesion from the force-field level, which superficially compares dielectric models to experimental results from the literature and suggests a method by which adhesive tendencies may be either anticipated or indexed. This work was initiated with the purpose of generating a re-perspective of adhesion from the molecular level in support of future composite and adhesives research. This project was funded by Independent Research funds of the Naval Air Warfare Center Weapons Division.

The report has been reviewed for technical accuracy by Dr. Geoffrey Lindsay.

Approved by
R. L. DERR, *Head*
Research Department
27 April 1994

Under authority of
D. B. McKINNEY
RAdm., U.S. Navy
Commander

Released for publication by
S. HAALAND
Deputy Commander for Research and Development

NAWCWPNS Technical Publication 8152

Published by ..... Technical Information Department
Collation ..... Cover, 19 leaves
First printing ..... 40 copies

REPORT DOCUMENTATION PAGE

Form Approved
OMB No. 0704-0188

1. AGENCY USE ONLY *(Leave blank)*	2. REPORT DATE	3. REPORT TYPE AND DATES COVERED
	April 1994	June 1993-February 1994

4. TITLE AND SUBTITLE
Dielectric Models in Adhesion and Extrapolations of Molecular Modeling (U)

5. FUNDING NUMBERS
Work unit 1130504
Element 61152N
Task ROONO
Program 1117 14

6. AUTHORS
Nancy E. Iwamoto

7. PERFORMING ORGANIZATION NAME(S) AND ADDRESS(ES)
Naval Air Warfare Center Weapons Division
China Lake, CA 93555-6001

8. PERFORMING ORGANIZATION REPORT NUMBER
NAWCWPNS TP 8152

9. SPONSORING/MONITORING AGENCY NAMES(S) AND ADDRESS(ES)

10. SPONSORING/MONITORING AGENCY REPORT NUMBER

11. SUPPLEMENTARY NOTES

12a. DISTRIBUTION /AVAILABILITY STATEMENT
Approved for public release; distribution is unlimited.

12b. DISTRIBUTION CODE

13. ABSTRACT *(Maximum 200 words)*

(U) In order to separate mechanical mechanisms of adhesion such as surface roughness, chain entanglement, or even chemical reaction from mechanisms based upon the dielectric nature of interface interaction, highlights of dielectric theory dealing with cohesion and adhesion are reviewed. Elements of those theories are applied in order to gain insight into experimental results of adhesive systems taken from the literature. From this analysis dielectric-based explanations are offered for general adhesion trends, including explanations of metal to nonmetal adhesion trends based upon properties of the changing metal and the constituents of the interface. An example of how a dielectric-based explanation could be used to rationalize contributions from both the interface compositions and bulk components is also given. Finally an example of dynamic molecular modeling is given in order to compare current computer models of adhesion.

14. SUBJECT TERMS
Adhesion, Adhesion models, Adhesive, Cohesion, Dielectric constant, Thermal conductivity

15. NUMBER OF PAGES
36

16. PRICE CODE

17. SECURITY CLASSIFICATION OF REPORT	18. SECURITY CLASSIFICATION OF THIS PAGE	19. SECURITY CLASSIFICATION OF ABSTRACT	20. LIMITATION OF ABSTRACT
UNCLASSIFIED	UNCLASSIFIED	UNCLASSIFIED	UL

CONTENTS

INTRODUCTION

The problem of categorically defining and calculating exact molecular contributions to adhesion and cohesion in terms of elementary forces has always been difficult because of complications arising from exact definition of the interaction surface and the correlation to actual data. In addition, the scale of the practical problem often creates difficulties in diagnosing or separating the procedural from the chemical or molecular scale variables during adhesion formation. Complications range from surface roughness, dielectric contamination, and adsorbed surface fluids and semi-fluids, to the determination of all of the specific molecular entities and orientations as well as their pertinent dielectric properties involved in the adhesive event (References 1 through 8).

Some of these problems are simplified by newer methods of probing surfaces such as the surface force apparatus and atomic force microscopy (Reference 9 through 24). Such techniques may scan both laterally for changes in their dielectric properties and vertically for measuring minute attractive forces. Depending upon the structure probed, the interpretation can be a straightforward analysis of the dielectric forces involved. Disregarding the factors due to purely mechanical structures (formed from surface roughness, chain entanglements, interpenetrating networks, bond formation, or chemical reactions), adhesive forces can be described in terms of the dielectric mechanisms at work.

This analysis attempts to probe some of the practical approaches to dielectric theory in terms of recent experimental data.

DISCUSSION SECTION

Mechanical mechanisms due to surface roughness, chain entanglements, and chemical reactions are known to dramatically enhance adhesive forces and form the basis of many adhesion enhancement techniques. However, if mechanical mechanisms were separated, the underlying adhesive mechanisms are dielectric in nature. Ignoring bond potentials, these mechanisms include orientational and inductive effects, dispersive Van der Waals, and electrostatic (or coulombic) contributions. Electrostatic and dipolar interactions have been reviewed by Bottcher (Reference 25) in terms of both average properties and statistical mechanics, and dispersive derivations have been reviewed by Israelachvili, McLachlan, and Voyuskii (References 10 and 26 through 29).

In general, the study of adhesion or cohesion involves the determination of energy loss mechanisms which enable the combined interfaces to stabilize over that of the individual surfaces. This general concept differs from bond description only in that the effect of the molecular property is of interest, instead of the atom. The underlying problem of defining the interacting states is contained in many surface state theories including

transition state theory, work function theories, electrostatic derivations, and basic theories of adsorption and adhesion (References 1, 2, 24, and 30 through 33). The energy states of interest may best be solved using quantum mechanics; however, this is often not practical. Dielectric analysis of the mechanisms brings about a more simplistic explanation of adhesion since quite often average properties are used. For many purposes, average properties are sufficient to describe the dielectric nature of the surface and interface. In this way the connections to bulk observable dielectric properties can be extrapolated, which is of the most practical use to the applications specialist. These can lead directly to molecular theories of adhesion and further relationships to measurable quantities.

Our analysis begins with examples of two specific interactions, the metal-dielectric interface and the dielectric-dielectric interface, and observations from experiments. Finally, dynamic contributions to the adhesive question will be questioned through examples of recent molecular dynamics calculations.

BACKGROUND CONCEPTS

Since polarity is considered a time averaged event, nonpolar molecules, as well as polar ones, can be found to possess a finite instantaneous dipole if studied within a short enough time domain. These moments induce a field in neighboring particles giving rise to an internal force or field. The instantaneous dipole components are called dispersive forces, whereas the orientational and inductive effects are reserved for the specific cases of polar molecules. In general, dispersive forces overshadow polar contributions except when the molecule exhibits specific dipolar or quadrupolar characteristics in the order that association occurs. The geometry of this association and its effects on the combined field often lead to unpredictable Van der Waals contributions. All of these mechanisms help to describe the molecular and atomic contributions to both adhesive and cohesive forces, which are mechanistically similar in origin on the molecular scale in terms of requiring an interacting electric field. Depending upon the scale of interaction, each of the contributing forces (dipolar and induced effects, Van der Waals dispersion, and electrostatic contributions) can be derived separately.

The energy of electrostatic interaction is defined as the work required to bring two particles from an infinite distance to within a distance (d). The derivation is specific for an interaction (if known) and has been reviewed by Bottcher (Reference 25) in terms of polarizabilities. It can generally be thought of as (where W = work):

$$W = \text{charge-charge} + \text{dipole-charge} + \text{dipole-dipole} + \text{self-induced moment interactions} \quad (1)$$

At long distances the charge-charge energy (proportional to 1/d) is dominant; at intermediate distances the charge-dipole energy (proportional to $1/d^2$) becomes dominant; at smaller distances charge-quadruple and dipole-dipole energies (proportional to $1/d^3$) are dominant; and at still smaller distances charge-octapole and dipole-quadrapole energies become dominant. Interaction geometry must also be taken into account. For example, for the specific example of two polarizable dipoles, electrostatic energy has been expressed by Bottcher as:

$$W \text{ (min, parallel, coaxial)} = [-2/(1-2a/d^3)][\mu^2/d^3]$$
$$W \text{ (antiparallel, coplanar)} = [-1/(1-a/d^3)][\mu^2/d^3]$$
$$W \text{ (max, antiparallel, coaxial)} = [2/(1+2a/d^3)][\mu^2/d^3] \quad (2)$$

where a = polarizability,
μ = dipole moment, and
d = distance.

Because of the assumptions used during derivation, which applies the results of large separations at very short distances where charge distributions overlap, it has been argued that quantum mechanics derivations should be used and are especially important for dispersive forces in condensed systems.

Van der Waals forces are quantum effects and have been derived using quantum theory in terms of two interacting systems. The result, which uses specific field tensors to describe the dielectric, reflects the impact of polarization, dielectric constant, frequency, and distance parameters (References 10 and 25 through 28). A generalized form of these derivations of the dispersive energy can be shown to be proportional to the polarizabilities (Reference 26):

$$W \propto 1/d^6 \int a(\omega)E(\omega)b(\omega)E(\omega)\, d\omega \quad (3)$$

where a and b = polarizability,
ω = frequency, and
E = electric field.

In general, the cohesion from Van der Waals forces is dependent upon the dipole moments and polarizabilities in the form of dielectric constant and frequency dependencies.

Dipolar effects such as orientational and induced effects arise from polarization due to a molecule's own internal field. It can also be derived in terms of instantaneous polarization for nonpolar entities. Such a field has been termed by Bottcher as the reaction field (R) and is described as the electric field due to the dielectric felt at a dipole induced by that dipole (Reference 25). This approach differs from an electrostatic one in that it can derive an average field based upon average properties such as dielectric constant and refractive index and has been called a continuum approach.

The reaction field is a function of the polarity of the dipole (μ) in general terms by:

$$R = f\mu \quad (4)$$

where f is a function of the reaction field describing cavity shape, size, and dielectric nature. The reaction field can also be described in terms of the total moment of the dipole in an energy field (m), which then includes contributions from both the permanent (μ) and induced components (p) and where a is the scalar polarizability, and E is the electric field:

$$R = fm \quad (5)$$

where $m = p + u$; and

$$p = aE \tag{6}$$

The exact nature of the reaction field will depend on the exact nature of the dipole and cavity, such as its polarization potential and shape, as suggested by Equation 4. For example, the reaction field of a polarizable dipole in a spherical cavity has been given as (Reference 25):

$$R = (4\pi/3)N[2(\varepsilon - 1)/(2\varepsilon + n^2)][(n^2 + 2)/3]\,\mu \tag{7}$$

where ε = dielectric constant,
n = refractive index, and
N = number of particles.

In general, the presence of the reaction field effectively increases the dipole moment of the dipole, and has been described to contribute to the cohesion of polarizable particles. The energy of cohesion (W) has been given in terms of the reaction field as:

$$W = -1/2\,\mu \cdot R \tag{8}$$

which is the work required for a permanent dipole to be surrounded by a dielectric; or for a system of identical molecules:

$$W = -1/2\,N\mu \cdot R \tag{9}$$

(where the higher the absolute value of Equation 4, the higher the cohesion energy). Taken together with the reaction field, the energy is proportional to μ^2 (or the m^2/d^n, depending upon the reaction cavity description), the dielectric constant (and wavelength dependence), and the refractive index. Therefore, any mechanism which increases the susceptibility will increase the reaction field, and the energy involved in surrounding the dipole in the dielectric. The total reaction field depends upon integration over all of the particles involved. Because of this, density, size, and shape factors could be incorporated into the overall expression. Bottcher has also compared Van der Waals contributions by calculating the difference in vaporization energy with ideal gas and dipolar effects (Reference 25). However, McLachlan questions the use of cavity fields to explain dispersive forces (Reference 26).

The dielectric nature of the interaction is not easily solved by first principles because all of the contributing interaction configurations must be known. However, it appears that the stabilization will increase with increasing dipole moments and polarizabilities of the constituents, as suggested by Equations 1 and 2. On the average, this will in turn be related to the individual dielectric constants, and refractive indices, as suggested by the relationship between dipole moment and dielectric constant in Onsager's equation. For example for spherical molecules:

$$\mu^2 = [9kT/4\pi N][(\varepsilon - \varepsilon_\infty)(2\varepsilon + \varepsilon_\infty)]/[\varepsilon(\varepsilon_\infty + 2)^2] \tag{10}$$

(This has also been derived in a more general form for ellipsoidal molecules showing the shape effects of the dipole on its moment (Reference 25).) A more specific derivation of the molecular structure contribution to the macroscopic properties is given by statistical mechanical approaches. These have led to generalized derivations of the Onsager's equation, such as the Kirkwood-Frohlich equation:

$$g\mu^2 = [9kT/4\pi N][(\varepsilon - \varepsilon_\infty)(2\varepsilon + \varepsilon_\infty)/\varepsilon(\varepsilon_\infty + 2)^2] \quad (11)$$

where g is a correlation factor relating the intermolecular interactions.

METAL-DIELECTRIC ADHESION

A very common and practical problem is the prediction of the adhesion of metal to dielectric surfaces. Examples range from paints to semiconductor circuits. The difficulty in describing the adhesive or cohesive bond stems from the macroscopic entities often used to describe the event. However as mentioned above, disregarding mechanical and direct covalent bond contributions, dielectric mechanisms may be separated and understood at a molecular level.

For a metal to dielectric adhesive bond to be stable, the total energy of the system must effectively decrease, which is true of any stable interacting system. Remember that the reaction field of a dielectric is a function of the susceptibility of the molecular components and their geometrical interactions. The interaction at the interface can then be given as a function of the interacting electric fields. For stability at the interface of an adhesive system, the energy loss mechanisms will then become a function of the surface geometry, as well as molecular structure. In addition, the continuity or discontinuity of these fields may determine or alter the important mechanisms involved during the adhesive event and failure. For instance, it is known that polymer structures at the interface of metal-polymer surfaces differ from that of the bulk (References 3, 4, and 34 through 44). For polymers, this may be because of changes in the surface structure from discontinuous symmetry constraints compared to the bulk (References 34 and 43 through 46) or energy and chemical changes at the surface (References 3, 4, and 36 through 41). For metals, changes in surface structure because of deposition conditions and surface treatments has also been of concern for adhesion (References 3, 4, and 35 through 42). Both the work-force anisotropies (References 1 and 30 through 32) and transition state theories must contend with functions of the surface structure and so must also be related to the interacting electric field. In this way, charge differentials may theoretically be stabilized either across a larger surface area leading to low surface fields or across a smaller one leading to high fields.

The metal to dielectric reaction field may be simplified because the metal has an additionally important mechanism compared to the dielectric, owing to accessible conduction bands. These include both electric and thermal conduction mechanisms which describe electron movement or scattering. Theoretically then, such mechanisms could contribute heavily to the energy loss pathways of the metal-dielectric interface and may be especially important when comparing different metal adhesion to similar dielectrics.

Under the assumption that the loss mechanisms inherently present for the conductor will contribute as much as the dipolar mechanisms of the dielectric, a simplistic argument can be drawn based upon basic electronic principles and average properties. Consider that the metal-dielectric surface is analogous to a capacitive circuit. The energy loss within a capacitive system upon charging is classically related before and after introduction of the dielectric to:

$$\Delta E = (1/2)C_0V_0^2 - (1/2)CV^2 \qquad (12)$$

where C = capacitance = εC_0,
V = field strength with dielectric = V_0/ε,
ε = dielectric constant,
C_0 = free space capacitance = $\varepsilon_0 A/d$,
V_0 = applied field strength without dielectric,
ε_0 = free space permittivity,
A = area of capacitor surface, and
d = distance between capacitor plates.

The loss mechanisms in the capacitive circuit stem from the change in dielectric constant from air and the effects on the apparent capacitance and field strength. From this simplistic model, argument can be made that the material properties contained in the second term determine the relative energy loss of the system.

Using what could be termed a phenomenological-continuum approach, the electric field for a target polarizable element of a dielectric in a metal-dielectric interface could arise from the reaction field of that dielectric. This model can be visualized using a discontinuous surface so that upon metallization, the metal-dielectric interaction can be considered as a series of capacitors. For simplicity, assume that the surface field is an extension of the bulk reaction field (R). Assume also that metal contact occurs without any further deformations of the surface. After metal contact, the capacitive circuit is formed; the analogous charging of the capacitor will take place under the influence of the reaction field. The energy loss mechanisms will analogously be related to the properties of the circuit such as the resistivity of the metal. The loss mechanisms can now be related through classic mechanisms. For the moment, ignoring initial states, the energy E at the target element (n) is:

$$E(n) = -(1/2)CV^2$$

Expanding to the electrical equivalents:

$$\begin{aligned} E(n) &= -(1/2)i^2pt \\ &= -(1/2)q^2pt \\ &= -(1/2)C^2V^2p\omega \\ &= -(1/2)\varepsilon^2C_0^2V^2p\omega \\ &= -(1/2)\varepsilon^2\varepsilon_0^2[A/d]^2R^2p\omega \\ &= -(1/2)\varepsilon^2\varepsilon_0^2[A/d]^2R^2\omega L/K \end{aligned} \qquad (13)$$

where i = current,
p = resistivity of metal,
t = seconds,
A = area of surface dipole "capacitor" element,
d = distance between dipole surface elements,
ω = frequency (or time domain of conductivity),
R = reaction field of the dielectric,
ε = dielectric constant of the dielectric,
ε_o = permittivity constant,
L = Wiedeman-Franz constant of the metal,
K = thermal conductivity of the metal, and
q = coulombs.

This will be related to the energy loss of the total system, but may be particularly useful in predicting the trend of different metal to similar dielectric adhesion. Interestingly, it appears that in the quantum derivation of McLachlan in which the dispersive energy of a condensed rather than a gas phase was derived, field tensors were used, which reduced the free space field by a factor equivalent to the medium's dielectric constant (Reference 26 through 28). From a macroscopic scale, this is analogous to a capacitor of an electronic circuit decreasing the free space field by a factor equivalent to the dielectric constant.

In reality, this simplistic picture will be complicated by the actual composition and geometry of the molecular scale metal-dielectric interface in which case field tensors will replace the simple reaction field. For example, the surface field will differ from the bulk because of discontinuities from the bulk in the reaction field and adhesion changes have been identified due to metal surface roughness as well as dielectric surface changes (References 3, 4, 17, and 35 through 42). Exact solutions of the surface reaction field will depend upon exact definition of the size, shape, and polarizabilities of the dipole element and upon the effects of the surface shape. Theodorou has devoted a body of work to the definition of the surface interfaces using lattice models (References 45 and 46).

Simple experimental evidence appears to support the general validity of Equation 13. For instance, the observed adhesion order of metal films deposited at room temperature or at low temperatures on polyethyleneterpthalate (PET), as measured by Silvain and others (Reference 34), fits reasonably well with its resistivity and inverse thermal conductivity (Table 1). From this work, metal adhesion to PET decreases Mg > Al > Ag > Cu; whereas resistivity decreases Mg > Al > Cu $\geq$ Ag. Interestingly, the inverse thermal conductivity at low temperatures shows the best agreement with the adhesion data, with Mg > Al > Ag > Cu, which suggests structurally influenced adhesion changes. For instance in both the adhesion data and the thermal conductivity data, anomalous behavior occurs for silver between the low temperature and room temperature trends. This behavior may indicate similar sources of mechanistic changes for this metal, such as surface structure changes induced by the deposition conditions which are known to occur (References 3, 4, 17, and 35 through 42).

TABLE 1. Resistivity and Thermal Conductivity of Selected Materials.

	Thermal conductivity, watts/meter-Kelvin[a]		Ideal resistivity, micro-ohm-cm[b]		
Metal	273 K	77 K	300 K	273K	80 K
Mg	153	200	4.51	4.05	0.557
Al	235	440	2.733	2.417	0.245
Ag	428	481	1.629	1.467	0.289
Cu	401	610	1.725	1.543	0.215
Au	318	354	2.271	2.051	0.481
W	170	264	5.44	4.82	0.606
Ti	22	33	...	39.0	0.48
Zn	119	138	...	...	...
Graphite (natural)	160	610	65 (RT)	...	...

[a] Reference 47.
[b] Reference 48.

From the experimental results of Silvain and others, as the substrate deposition and process temperatures increase, anomalies begin to appear in the form of drastically increased adhesion at room temperature, independent of the metal (Reference 35). This anomaly may be explained by a change in the interface structure. For instance, if oxidation of the metal were to occur at the interface, the apparent dielectric constant of the polymer interface would increase, due to higher dielectric contributions from the metal oxide. Equation 13 would then predict an enhanced adhesive bond from enhanced capacitive effects, dielectric constant, and from an enhanced reaction field.

The most recent support of metal mechanisms directly involved in adhesion has been found in the semiconductor area. Dr. Paul Kohl at Georgia Institute of Technology, Atlanta, recently found that thin layers of titanium oxide of not less than three angstroms promoted adhesion of gold, silver or copper to silicon dioxide and polymers (reported in "Semiconductor International," Reference 49). This advent would allow replacement of aluminum in integrated circuit manufacture by more conductive, but less adhesive metals. The layers are formed by metallization with subsequent oxidation so that the oxide would sit on top of a layer of titanium metal. In agreement with Equation 13, the higher adhesion could be argued from both the higher dielectric constant of titanium oxide (100 - >1,000, Reference 47) and from the higher resistivity and lower thermal conductivity of titanium. From the trends in the electrical properties, titanium metal would be expected to have greater adhesion to silicon dioxide or polymer than adhesion of the silicon oxide to gold, silver, or copper. In addition from Equation 13 and the relative dielectric constants, titanium dioxide should have greater adhesion to gold, silver, or copper than to silicon dioxide. The sandwiched adhesion promotion of the titanium and titanium dioxide appears to be very predictable when extrapolated from their relative properties.

In fact, previous investigations have shown that metal oxides and other compounds such as carbides, nitrides, and organometallic species form at the metal-polymer interface

depending upon process conditions and contribute to adhesion (References 3, 4, and 35 through 42). These conditions, which include thermal treatments as well as plasma and chemical modifications, alter the definition of the dielectric surface to be used as applied to Equation 13. Other studies indicate that migration of polar species to the surface contributes to adhesion (References 35 and 37). In either case, the existence of such layers serves to increase the dielectric constant of the apparent polymer interface which in turn increases the adhesion tendencies. The surface shape factors may become very important if conditions allow generation of a high reaction field due to specific surface orientations, alignments, or discontinuities, which encourage high field differentials.

Even though the evolution of this model is not rigorous, it is significant as it begins to relate some of the macroscopic measurable events such as resistivity or thermal conductivity and dielectric constant, as well as shape factors (such as dipole shape and eventual statistical number when integrated to the total surface) and dynamic factors to the overall expected adhesive property of the metal-dielectric interface. The shape factors will become evident and predictable as more research into the effect of molecular structure on the fractal nature of surface shape evolves (which leads to better definition of the surface reaction field). For instance, alignment of elements at the surface would be expected to create a high dipole density, and better adhesion is predicted. This has been experimentally studied by the increased adhesion in oriented liquid films between two solid substrates (References 13 through 15). Frequency considerations have already been mentioned in previous analyses of Van der Waals forces and are dependent upon the dielectric constant, refractive index, and density (References 9 through 15 and 26 through 29). Other possible mechanisms may occur through lattice and bond contributions (bond vibration, rotation, and translation or orientation) and must also be included for refinement and include both the metal and dielectric sides of the interface. So, Equation 13 is a simplistic model of the metal mechanisms and must be refined for field shape effects. In addition, a further refinement would specifically add the effects of both the electrical and thermal conductivity as well as dielectric variables to the loss expression.

$$E_{loss} \alpha \sum f(\varepsilon, shape, p, \omega, R, K, N, T, dielectric) \quad (14)$$

The relationship between resistivity, inverse thermal conductivity, dielectric constant, and adhesion is interesting because it indicates that the loss mechanisms, which contribute to adhesion, are inherently due to metal lattice mechanisms coupled with dielectric mechanisms. Given similar dielectric surfaces, it appears that higher metal resistivity and lower metal thermal conductivity produces better adhesion, which indicates that energy transfer into the bulk metal (through thermal or electric conduction) does not help the adhesive bond. In other words, the energy loss mechanisms are localized. This makes sense if the metal-dielectric adhesion can be thought of only as an interacting field phenomenon, as in the quantum derivations by McLachlan. Generally, the difference between average field and quantum mechanical approaches can be qualitatively described in terms of the derivations and treatments of the electric field. Mechanistically, the resistivity at a given temperature is thought to consist of electron scattering mechanisms through lattice vibration and is temperature dependent. (A temperature independent term also exists, but will not be considered at this simplistic level.) Reduced resistivity or enhanced electric or thermal conductivity implies that low electric fields are required for conduction. This in turn implies lower energy barriers to electron flow or scatter, or lower kinetic energy. Low electric fields imply a lower stabilization energy from Equation 13; conversely, increased

electron flow by definition decreases the probability of field formation in the capacitive element of the dielectric suggested in Equation 13 leading to lower stabilization energy (Equation 13) to the adhesive bond. From the dielectric perspective, high metal conductivity implies lower energy or lower kT contribution at the interface; and from Onsager's equation (Equation 10) low kT contribution implies lower dielectric dipole moment which leads to lower adhesion. Mechanistically then, low resistivity creates a low probability of system work contributing to the reaction field and to the adhesion energy. High resistivity or low conductivity implies that a higher electric field is necessary for conduction, and higher kinetic energy is required to overcome thermodynamic barriers against electron flow. Analogously, this implies higher interaction dipole moments and higher adhesion, but also implies that the system must do work in order to sustain the fields which contribute to adhesion at the metal-dielectric interface.

As mentioned above, a simple approximation for the surface reaction field, may be derived using the reaction field of the bulk. For comparisons of different metals on the same polymer surface, this approximation may be adequate. For exact solutions, or for comparisons of different dielectrics, the fit of the approximation may depend upon the surfaces in question and the differences in surface structure, but to a first order will depend upon the strength of the reaction field R. In addition, this treatment considers only one polarizable element; for completeness, the energy must be integrated over the entire surface and which will necessarily then include functions of the changing dielectric surface and its topography. In this analysis, work-force energy has not been included, but could heavily contribute depending upon the reaction field strength generated at a specific site. This may be of specific importance in piezoelectric generating structures where the local fields become high enough to induce current production during deformation. Deformation as a part of the field equation becomes obvious when viewed from the dipole, as changes in macroscopic deformation must necessarily induce rearrangement of component dipoles.

Atomic force microscopy shows another clue as to the dielectric nature of the adhesive bond (References 16 through 21). In one experiment, dielectric capacitance between a tungsten tip and polymer versus silicon surfaces were explored. The measurements, during which the tungsten tip was scanned at an equi-potential surface demonstrated an increase capacitance gradient with the higher dielectric constant material. From Equation 13, an increase in capacitance gradient and dielectric constant suggests an increase in the force. This suggests an increase of the adhesive force between the tip and substrate, with the force greater for the silicon surface than the polymer surface.

Other surface force experiments using tungsten tips with various substrates demonstrate that Van der Waals attractive forces are dependent upon dielectric type. For instance in the work of Burnham and others, atomic force microscopy indicated a definite affect of the dielectric on the adhesive forces observed (References 19 through 22). This can be directly compared to work done by Israelachvili, Tabor, and others using surface force apparatus on mica, liquid, and gel surfaces, where the initial loading attraction was used to measure direct Van der Waals contributions (and confirmed $1/d^2$ nonretarded and $1/d^3$ retarded contributions predicted by London and Lifshitz) (References 9 through 15). However, higher surface forces were found using the smaller scale atomic force microscopy and have been attributed to work force anisotropies (Reference 24). This may be an interesting side effect of the ability of atomic force microscopy to sample the local dielectric field, instead of the average field.

The atomic force loading curves indicated a surface attraction to the tungsten tip with the apparent adhesion decreasing: alumina > stearic acid > polytetrafluoroethylene (PTFE) (Reference 20). The trends upon loading agree with general dielectric (Table 2) and polarizability differences among the different surfaces (assuming that the major interface exists between the tungsten and the probed surfaces) according to Equation 13.

TABLE 2. Dielectric Constants of Selected Materials.

Surface	Dielectric constant
Alumina	4.5-8.4[a]
Mica	6.6[b]
PTFE	2.0[a]
Stearic acid	2.3[a]
Diamond	5.5-5.7[b]
Silicon	11.7[b]
Cu(I) oxide	7.6[a]
Cu(II) oxide	18.1[a]
ZnO	8.14[a]

[a] Reference 48.
[b] Reference 47.

Since fluorinated stearic acid is expected to have a slightly lower dielectric constant than stearic acid when extrapolated from general known halogenation trends of hydrocarbons and polymers (References 25 and 48), the following adhesion trend was expected: mica $\geq$ alumina > stearic acid > trifluorostearic acid > PTFE. In agreement, the observed attractive force measured by atomic force microscopy decreased: mica > alumina > stearic acid > trifluorostearic acid > PTFE (Reference 20).

During the surface force experiments described above, loading was increased to obtain compression of the surface before unloading (Reference 20). (This is not an unlikely simulation for the study of the formation of normal adhesive bonds, since in the practical case compression is always used.) The unloading hysteresis was then recorded.

Given the above mechanisms, two factors exist which create the expectation for hysteresis behavior to be exhibited upon unloading in the atomic force experiments presented. First the samples were loaded into compression, which as described below would necessarily change the adhesive contribution. Second, the contributing attraction surfaces sampled during loading (even if not taken to compression), would not necessarily be the same during unloading because of the presence of pre-adhered layers. This effect will be described in the next section.

We can expect that upon compression the definition of the surface will be transformed. This has been discussed previously for adhesion by Israelachvili (References 2 and 9 through 15), as well as modeled (References 22, 50, and 51). The transformation

mechanisms in the dielectric will be both physical and chemical in origin and dynamically would include the following mechanisms: bond rotation and vibration, dipole reorientation, migration (for more mobile molecules) or translation, charge transfer, and even reaction. Because all of these processes are energy expending, it is possible to increase the adhesive energy (energy required to separate the tungsten tip from the surface) over that of the simple attractive forces. Without an external force or directing energy, internal field effects would help direct reorientation, translation, or migration of interacting dipoles to decrease interface energy. Under compression, the first order change is local deformation resulting in an increase in surface area interaction. The enhancement of interacting surface area will be an energy expending event in order to deform the surface and bulk, which is supplied by the work of compression. However the enhancement of the adhesive force apparent upon retraction of the tip, will be derived by the accumulation of additional field interactions within the increased surface area or interaction area. The energy changes are treated by the Johnson-Kendall-Roberts (JKR) adhesion theories, which are based upon contact area and the surface energy of reversible work (References 2, 33, and 34). From experiment, the adhesion order does not change, although maximum unloading force or adhesion is increased in each case because of increased surface contacts. From Equation 13, increase in surface contact affects adhesion by the increase in the number of contributing reaction field elements.

Increase in surface contact also suggests the relationship between adhesion and the cohesive forces which contribute to bulk modulus, since the bulk must also be deformed to increase the surface area of contact. Note, however, the bulk modulus cannot contribute to the interface adhesive force, since its only contribution is from the surface area interaction during loading. In addition, because contact time has also been shown to be a variable for adhesion, bulk properties will also affect and help determine deformation rates (Reference 2). Furthermore, the relationship to bulk properties during this change in the interaction surface will be related to the physical dynamics that are allowed, that is bond rotation, vibration, translation, dipole reorientation, migration, and even reaction. Some of these processes affecting bulk properties have previously been studied using molecular dynamics (References 52 through 55).

However, for the simple metal-dielectric interface, once the chemical nature of the interface is known, adhesion will depend mainly on the geometry of the surface with respect to the electrical properties of the metal in question and the dielectric nature of the individual polarizable elements of the dielectric. On a molecular scale, orientation of the surface with respect to individual dipole moments of molecules, ions, segments, and even bonds may be used if known. The most exact solution would involve description of all individual dipole moments (instantaneous and permanent) and their induction effects. However, most often, average macroscopic properties such as the dielectric constant, conductivity, and resistivity are the easiest to identify, and to a simple approximation would represent a surface average. Until exact surface interfaces are known, such rules of thumb may be used to obtain adhesive trends or tendencies rather than absolute force predictions.

Interestingly, from Equation 13 if the adhesion between a metal and dielectric were to increase, the following parameters must increase or be affected: resistivity, dielectric constant, capacitance, dipole moment, area of interacting dipoles, inverse distance between interacting dipoles, dipole density, inverse conductivity, and inverse thermal conductivity.

In the experimental examples given here and in the next section, almost all of these effects can phenomenologically be shown as contributors to the adhesive force.

DIELECTRIC-DIELECTRIC ADHESION

The reaction field induced by a dipole surrounded by a dielectric of a different species is similar to the pure component, except that inclusion of cross terms must be included to describe the interaction of the various species.

The total work described for a system of interacting reaction fields where the interface is described only by the interacting dielectrics may be analogously extrapolated from the cohesive case using average properties (Reference 25):

$$W \propto -1/2\, u_a \cdot R_b - 1/2\, \mu_b \cdot R_a \qquad (15)$$

In general, any or all mechanisms which serve to increase the reaction fields can also serve to increase this adhesive strength, as long as the polarization vectors do not increase (instead of decrease) the total energy of the interface upon interaction (Reference 25). From Equations 7 and 15, the mechanisms occur through the dielectric constant, refractive index, and dipole moment. Onsager's equation becomes significant as it demonstrates that the contributions to the dipole moment originate from both the static and high field dielectric constants. Structurally, those molecules with high dipole moment and polarizability would be expected to have higher adhesive characteristics than those of nonpolar character. In addition since the dielectric constant increases at or near a resonance, those structures with heavy imaginary components (such as broad-band absorbing structures and dielectric semiconductors) would be expected to have better cohesive or adhesive attraction in general. This is especially important when considering that the classic Van der Waals forces (proportional to $1/d^6$) are consistent only within distances close to $\lambda/2\,\pi$, where λ is an absorption wavelength. (The relationship between resonance and adhesion may also help explain modulus enhancements of composite structures such as graphite fiber-filled epoxies in which the non-polar character of the filler would not normally be expected to enhance properties but whose dielectric properties such as a high resonance over a large frequency range predict good adhesion.)

For a dielectric within a low to moderate electric field, three molecular mechanisms are important (Reference 25): (1) the electronic effects which are directly related to electronic transitions, (2) the nuclear or ionic effects which are directly related to bond and charge displacements through changes in bond lengths and directions, and (3) the lattice effects which originate through deformation and thermal responses of the bulk such as through molecular orientation, rotation, and translation mechanisms. These mechanisms represent possible direct responses to the reaction field and so contribute to the adhesive bond. The electronic and nuclear effects have briefly been alluded to by their relationship to the dielectric constants.

An example of direct lattice and nuclear effects can be found in the electro-optic effect, which relates changes in the local dielectric environment to macroscopic optical events. Such mechanisms may not necessarily enhance the interface adhesive bond unless they are involved in actively changing the dipolar mechanisms and enhancing the local

electric field effects (through alignment, orientation, crystallization, charge separation, etc.). However, lattice effects may also be implied through the effects of temperature. The extent of the reaction field as suggested by Equations 4, 7, and 10 is proportional to dipole densities through N, the number of dipoles or particles. This suggests that for the dielectric, an increase in temperature decreases N through thermal expansion effects which are directly related to lattice responses to temperature. Expansion should decrease the interacting reaction fields (Equation 7), decreasing adhesion. This trend phenomenologically agrees with general surface tension trends where generally the surface tension decreases with increasing temperature (below a critical temperature) (Reference 5). According to the JKR Theory, a decrease in surface tension or surface energy predicts a decrease in adhesion (References 2 and 32), and both models (Equation 7 and JKR Theory) are consistent with one another.

As mentioned before, for a stable adhesive interaction, the interacting surfaces must lose energy relative to their free surfaces, or work must be done by the surface. For metal-dielectric interfaces, obvious parallels to electronic pathways can be rationalized for metal and dielectric interaction at the surface. For dielectrics, mechanisms will be dependent upon the dielectric type and its specific properties. In general, for small distances within Van der Waals radii, the work of adhesion is associated with the movement and interactions of electrons. On an ideal surface, this has been found experimentally where the force laws change from retarded to nonretarded at distances above $\lambda/2\ \pi$; that is, the attractive Van der Waals are larger at distances near a resonance because of electric field interaction.

Surface force data has been used to confirm the Lifshitz theory of Van der Waals distance criterion (proportional to $1/d^6$) using a surface force apparatus by way of interacting mica surfaces (References 9 through 11). However, more importantly, surface force data has been used to characterize the adhesive nature of different dielectric species on substrates such as mica. Interesting work has been done by Horn and Israelachvili (References 12 and 13) and more recently by Allara and Nuzzo (References 14 and 15) on the adhesion forces of organized liquids on and between solid dielectric surfaces using surface force analysis. The oscillatory behavior observed in the force-distance curve has been described because of the tendency of semi-ordering of liquids on surfaces and the disruption of that order. These oscillations are understood theoretically and depend upon liquid shape, size, and distance, under the influence of the Van der Waals potentials of the surface. Interestingly, the greater the order, the greater the solvation force between the two layers. This may not be surprising when considering that energy must be expended to re-orient molecules for best surface packing; and any loss of entropy is more than recovered by the loss of energy upon formation of a large extended Van der Waals interaction. Therefore, in agreement with the model of adhesion discussed above, the ordering of the liquid at the surface should increase its affinity or adhesion for that surface because of the energy loss mechanisms used to obtain some order of the surface molecules.

The atomic force data of Burnham and others, previously discussed, presents an example of complications arising because of a dielectric-dielectric interface (Reference 12). Because of changes in the surface dielectric constant due to contaminations (or even reactions) at a metal-dielectric interface, the location of failure of the adhesive bond might actually be due to a dielectric-dielectric interface. The surfaces studied by Burnham (Reference 20) were much more complicated than suggested above for a metal-dielectric interface since the entire composite actually consisted of layers of interacting dielectrics as

shown in Table 3. Because of this, the unloading curve would consist of contributions of the tungsten-dielectric surface, the alumina-aluminum surface and the dielectric-alumina surface. So for the stearic acid and trifluorostearic acid dielectrics (example B and C in Table 3), the differences in their attraction would be due to more than one interface. A failure in an additional surface would be predicted if no stabilization energy, or less stabilization energy resulted by the insertion of the extra dielectric.

TABLE 3. Expected Interface Structure of Atomic Force Microscopy Example.

Example	Layer structure	Dielectric constants in the dielectric layer
A	W-alumina-Al[a]	W-9-Al
B	W-stearic acid-alumina-Al	W-2.3-9-Al
C	W-trifluorostearic acid-alumina-Al	W-<2.3-9-Al

[a] W = tungsten, Al = aluminum

For instance, the tungsten-alumina interface is expected to have higher adhesion than the tungsten-stearic acid interface according to Equation 13. Ignoring crystalline lattice stability of the bulk and surface area increases upon compression, the alumina-alumina interface is expected to have higher cohesion than the stearic acid-alumina adhesion from the interacting moments suggested by the dielectric constants and Equation 15. The tungsten-trifluorostearic acid interface is expected to have lower adhesion than the tungsten-stearic acid interface; and finally the trifluorostearic acid-alumina interface is expected to be of lower adhesion than the stearic acid-alumina interface, again because of the interacting dielectric components of the reaction fields. This orders the expected total unloading work to be A > B > C, which is suggested by the trend in the actual atomic force data (Reference 20). Further derivation of the interacting reaction fields must still be derived in order to understand the extent of the failure at each surface.

Therefore, identification of energy loss and balance mechanisms become key to the understanding of adhesive properties. Such mechanisms depend upon the average properties such as the dielectric constants and wavelength dispersions of the components (which in turn depend upon the molecular structure), as well as the orientations of the surface which tend to balance energy and enhance specific interactions and the effects of the surface reaction fields. In addition, more macroscopic events due to dielectric responses (translation, rotation) could also be involved in failure mechanisms. This has been previously simulated using molecular dynamics which showed that movements induced between two polymers may actively lead to cohesive loss mechanisms (References 52 through 55). Modeling will be discussed in the next section.

A striking example and confirmation of the role of the dielectric properties to adhesion comes from the theoretical work of Porter (Reference 56) and the experimental work of Elwell *et al.* (Reference 57). Elwell verified the theoretical linear relationship between the peel strength of an adhesive bond and the dielectric loss of the adhesive. On the other hand, Ingo *et al.* (Reference 58) attributed different metal oxide to lacquer adhesion results from the semiconductor mechanisms of the oxide in which the localization of electrons and holes gives rise to the adhesion. From the interacting force field perspective, this could be considered as mechanistically similar to the dielectric argument.

In addition, the localization explanation of effects is similar to localization arguments given for metal-dielectric adhesion discussed above.

AN EXAMPLE OF THE CONTRIBUTIONS

To illustrate what the above contributions may entail, the case of a polymer bonded to a metal surface will be qualitatively considered. The total adhesion force will be a compilation of the metal-polymer, polymer-polymer, and any intermediate layers such as the metal-oxide and oxide-polymer layers.

The following expression may be visualized for the general interface interaction energies:

$$W \alpha \Sigma f(\varepsilon,A/d,p,w,R)_{metal\text{-}oxide} + \Sigma f(\varepsilon,A/d,p,w,R)_{metal\text{-}polymer} + \Sigma f(\mu,R)_{oxide\text{-}polymer} + \Sigma f(\mu,R)_{polymer\text{-}polymer} + \Sigma f(\mu,R)_{oxide\text{-}oxide} + \ldots \quad (16)$$

where all individual dipole elements may be defined in terms of significant dynamic geometrical interactions (References 52 through 55). Ideally, the chain orientational interactions must be taken into account at the interface in contact with itself and with the metal or metal-oxide. For instance in polymer blends, each different polymer-polymer and polymer-metal or polymer-oxide interaction and orientation should be weighted and considered as separate interface interactions.

For the metal-polymer example, these different distinctions become important since the higher number of interfacial contributors are associated with the polymer, the more likely the stress will be stabilized over a larger interfacial area (associated with chain interaction), and the higher the resulting adhesive force. The force distribution mechanisms must then be considered, as well as the chemical make-up and dipole populations at the various interfaces.

This is clearly demonstrated in the work of Packham *et al.* in which topographical contributions to the total adhesive force (References 59 through 61) were considered by creating an oxide surface on which to base the correlations. In Packham's work, changes in topography were explained as mechanical in nature; however, in this discussion these observations can also be explained using a dielectric instead of a mechanical mechanism. For instance for metal-epoxy interfaces, the higher the oxide surface area, the higher the adhesional force; however, upon rubber toughening of the epoxy the failure interface moved from the metal-oxide surfaces to the oxide-polymer interface. Both of these observations are clearly implied in Equation 16 which may be expanded as:

$$\begin{aligned} W \alpha\ & \Sigma f(\varepsilon_{oxide},p_{metal},R_{oxide}) + \Sigma f(\varepsilon_{epoxy},p_{metal},R_{epoxy}) + \Sigma f(\varepsilon_{rubber},p_{metal},R_{rubber}) \\ & + \Sigma f(\varepsilon_{epoxy\text{-}rubber},p_{metal},R_{epoxy\text{-}rubber}) + \Sigma f(\mu_{oxide},R_{epoxy}) \\ & + \Sigma f(\mu_{oxide},R_{rubber}) + \Sigma f(\mu_{epoxy},R_{oxide}) + \Sigma f(\mu_{rubber},R_{oxide}) \\ & + \Sigma f(\mu_{oxide},R_{oxide}) + \Sigma f(\mu_{epoxy},R_{epoxy}) + \Sigma f(\mu_{rubber},R_{rubber}) \\ & + \Sigma f(\mu_{epoxy},R_{rubber}) + \Sigma f(\mu_{rubber},R_{epoxy}) \end{aligned} \quad (17)$$

An increase in oxide surface area automatically implies higher number contributions from the oxide terms (that is summation over more molecular entities than with a low surface area interaction), which is consistent with the higher experimental adhesion of the fibrous oxide surfaces in comparison to the flat oxide surfaces. With the rubber additive, the forces are clearly distributed more into the polymer with less contribution from the oxide-metal interface alone, consistent with failure at the polymer-oxide interface. Redistribution of the incident stress over more interfaces via the mechanistically more deformable rubber creates a higher overall adhesive bond from the higher number of polymer interactions involved. Failure should therefore logically move into the polymer where the stresses are being redistributed. Analogously, localization of incident stresses using a less-deformable plastic such as epoxy (without rubber additives), must lead to failure at the interface closest to the oxide. In this case it is logically predicted at the oxide side of the interface with it's lower strain-to-break; this prediction is consistent with analysis which places fracture at the metal-oxide interface in structures without rubber additives.

In addition, in agreement with Equation 17 in which more entities are involved in adhesion, the rubber additive increases the total force required to separate the adhesive bond. This implies that for rubber-based adhesives the higher adhesive nature originates not only from higher intimate contact with the bonded interfaces or a higher interaction population (due to a higher flow probability from both the rubber and rubber-softened epoxy blend), but also from the higher bulk contribution of the rubber adhesive to the dynamics of adhesion. Bulk participation should then also increase the interaction population contributing to the total adhesion. The question of bulk participation into adhesive bond strength is implied in Equation 17, however Equation 17 also questions contribution balance. The above analysis implies that the important contributing interfaces differ not only by the strength of the field interaction but also by the populations of interactions rather than the magnitude of any single interaction; otherwise the higher modulus epoxy bond would exhibit higher total adhesional force in contrast to the epoxy-rubber blend instead of higher adhesion from the rubber toughened case. Low modulus rubber and rubber-based adhesives have high contributions to the total adhesion due to the ability to dynamically distribute the response mechanisms into the bulk increasing the total number of contributing interactions. This also begins to explain the household-tip of using ice to remove chewing-gum from fabrics. When cold, the gum-gum interactions increase in strength and the applied force cannot dissipate into the bulk of the material. Failure can be predicted to move to the wanted gum-fabric surface. Lower total number interactions at the interface automatically predicts a lower adhesive bond, and the gum is easily scraped off the surface of the fabric. This analysis implies that to increase the total adhesive force, the interface contributions must be balanced correctly to distribute the incident impulse away from the weakest interfaces; this distribution is inherent in Equation 17.

Implications may also be drawn as to the impact of the metal used. Without the rubber additive, where contributions from the oxide are high, higher significance of the oxide terms in Equation 17 are expected thus explaining the higher experimental adhesion of epoxy bonded to copper than to zinc (where the dielectric constant of copper oxide is twice that of zinc oxide). With the rubber additive, the adhesion to the zinc/zinc oxide surface showed higher experimental adhesion than to copper/copper oxide indicating mechanistically that the contributions to failure had moved relative to epoxy only results. This change may be argued from several dependent directions. For instance, creating a rubber blend creates an additional metal-dependent term in Equation 17. This additional

interface, depending upon population densities may increase the role of the metal through which thermal conductivity trends should emerge. This helps to explain the higher adhesion of the rubber blends to zinc than to copper (where the thermal conductivity of zinc is lower than that of copper).

On the other hand, it may be argued that by rubber toughening, the stress locations are distributed into the polymer bulk creating less dependence on either the metal-oxide or oxide-polymer interfaces alone. This re-distribution, suggests that interface population densities which are oriented to react in opposition to the applied force, will determine the relative significance of the different terms in the above equation. Although not directly apparent by Equation 17, this is a miscibility question; where generally it may be argued that the higher dielectric copper oxide surface would be more compatible with the higher polar epoxy surface due to the higher interactional energy possible. This enhanced epoxy interaction relative to the zinc/zinc oxide case would in turn destabilize the adhesive interaction by concentrating more relative stress at the brittle oxide-epoxy and metal-oxide interactions rather than distributing the stresses into the bulk, leading to failure early in the applied impulse. By analogy, the lower dielectric oxide (zinc oxide) may be considered to be the more compatible with the rubber component, leading to the observed trend. Generally, miscibility as well as diffusion issues will be more easily recognizable from interface aging issues than from the younger age effects, but must not be ignored if the correct interactions are to be considered and identified.

Similar implications may also be drawn about the type of metal oxide used as observed by similar adhesion trends for copper to polyethylene data (References 60 through 61), where higher adhesion to copper [II] oxide is observed than to copper [I] oxide. In this case the dielectric constant of copper [II] oxide is twice that of copper [I] oxide, consistent with the observed experimental trend. Failure in these systems occurs at the polymer-oxide side of interface showing how the higher deformable plastic tends to distribute the incident stresses over a larger area, which is in agreement with the rubber additive implications.

This example demonstrated that all dielectric forces involved (from dispersion to coulombic, from miscibility issues to adhesional issues, and even from shape to population issues) must be considered in order to adequately define the total experimental observations. Once categorically defined, simple extrapolations from the dipolar nature of the materials involved to the expected type of failure may be (at least) qualitatively derived. Mechanistically, it is important to realize, that once the stress distribution is understood (which will be a function of the type of dielectric interactions, shape, and bulk properties) it is easy to understand adhesional failure sources.

These contributions are further summarized in Figures 1 and 2, which compile the experimental data of Silavin *et al.*, Packham *et al.*, and Evans *et al.* (References 35 and 59 through 61) in terms of the components of Equation 13. The data has been separated into smooth or untreated metal surfaces (Figure 1) and treated or roughened metal surfaces (Figure 2) in order to help distinguish dielectric sources of adhesion from mechanical ones. The role of both the conductive behavior of the metal and the dielectric nature of the oxides and polymers is graphically demonstrated in Figure 1 which shows the general increase in adhesion with increase in dielectric constants and inverse thermal conductivity. As is evident by comparison of Figures 1 and 2, treatment of the metal surface to either roughen

or increase the fibrous nature of the oxide coating may qualitatively enhance adhesion for that specific experimental group, but also tends to scatter the trends as a whole, making correlations very difficult. This can be predicted directly from Equation 17 with an increase in the interactional populations. The scatter in the data is also understandable from the lack of either qualitative or quantitative statistical correction for the terms in Equation 17. However, as issues such as morphological differences are taken into account and qualified as a predicted interaction population, better correlation of adhesion should be possible. And, in order to understand future experimental results, qualification of these types of effects must be taken into account.

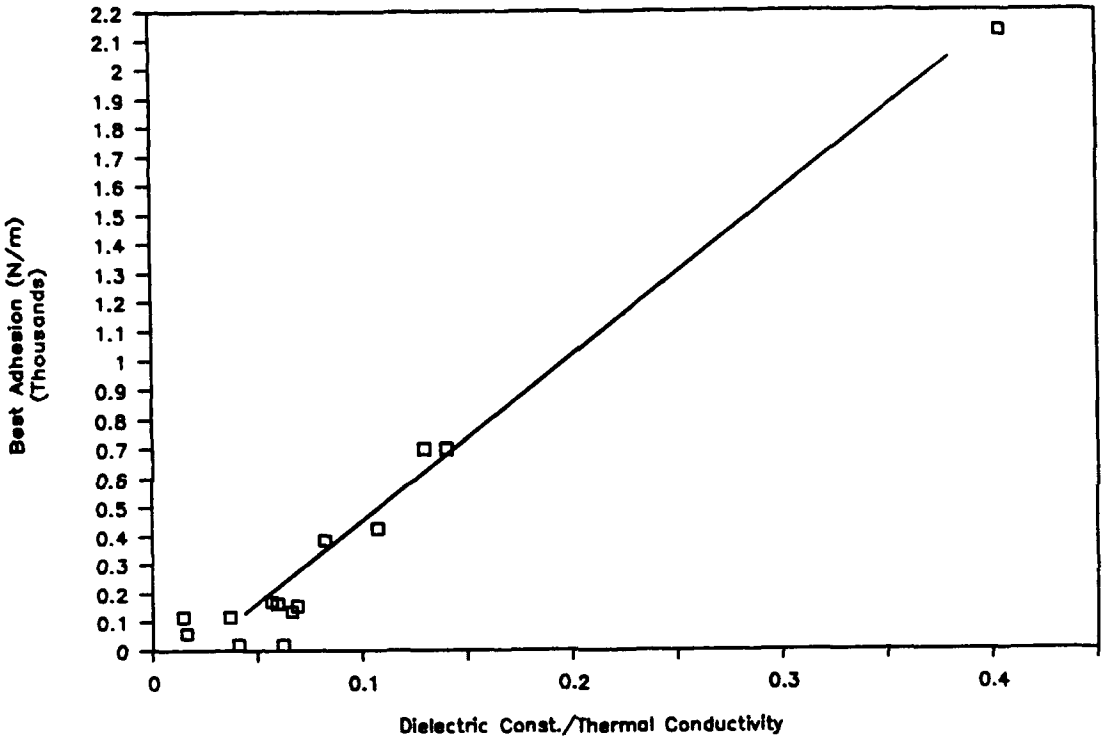

FIGURE 1. Best Adhesion (N/m) Versus Dielectric Constant/Thermal Conductivity ($\Sigma\varepsilon/K$) (from References 35 and 59 through 61 on smooth metal surfaces). Polyethyleneterephthalate, polyethylene, and epoxy on Mg, Al, Cu, Zn and/or steel are represented. Test type is ignored.

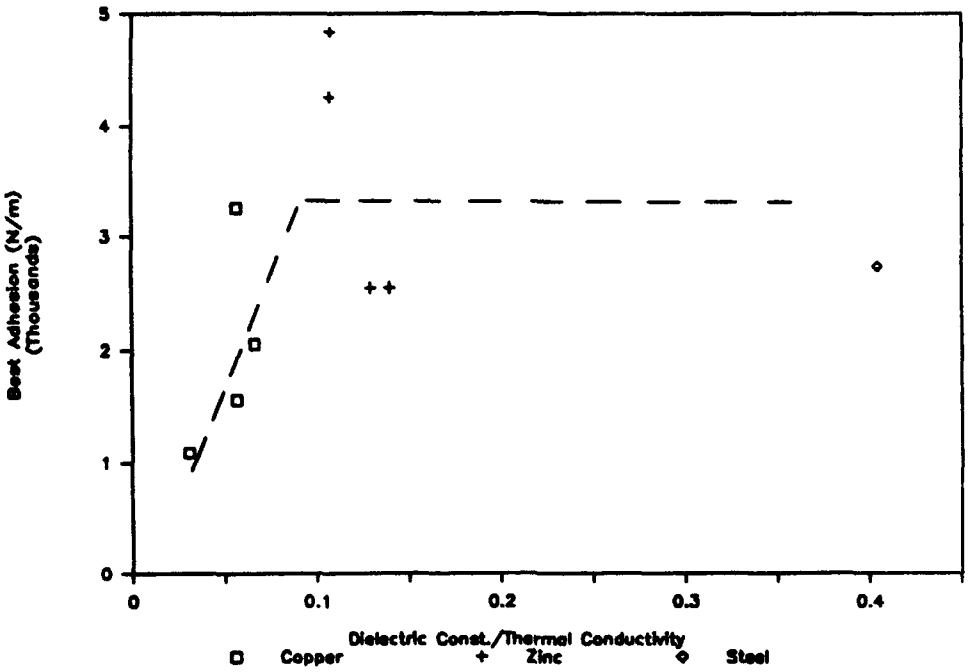

FIGURE 2. Best Adhesion (N/m) Versus Dielectric Constant/Thermal Conductivity ($\Sigma\varepsilon/K$) (from References 59 through 61 on treated metal surfaces). Polyethylenetherephthalate, polyethylene, and epoxy on Mg, Al, Cu, Zn and/or steel are represented. Test type is ignored (squares = Cu, crosses = Zn, diamonds = steel).

MOLECULAR DYNAMICS

Previously, it was argued that the exact definition of the interacting fields would be of utmost importance and would be material dependent. That is, the interaction field would need to be defined as combinations of either bond dipoles, molecular dipoles, chain moments, or even surface moments, depending upon the exact interaction geometries and populations. However, this is also made more complicated by motion at the interface because of thermal or deformation responses.

Therefore, dynamic pathways of obtaining adhesion are as important as understanding the adhesive force. For dielectrics, nuclear and lattice mechanisms may be used to expend energy by processes such as bond rotation, vibration, and even translation (Reference 25) and are often measured using dielectric relaxation techniques (References 25, 57, and 61 through 65). These techniques can sample electric field responses on a molecular level creating a better understanding of the effects of absorption by local fields. As discussed above, since enhanced interface reaction fields may contribute directly to energy stabilization, the understanding of field-field interactions leads to better understanding of stabilization pathways. Nuclear and lattice mechanisms could also be observed by temperature differentials in the materials or the effects of temperature on dielectric response which define any changes in kinetic energy. Therefore, transfer of

energy out of the interface in the form of heat, light, or work, automatically defines an increase in the adhesive force.

By contrast to experimental techniques, computer simulation of dynamic systems brings an added dimension from the ability to study adhesion or cohesion from specific effects of molecular and bonding structure, as well as extrapolations of rate effects and hysteresis (References 44, 50 through 55, and 66 through 71).

By this time, it may be apparent that cohesion and adhesion are very similar in origin, and that modulus and strength trends are basically similar to cohesional and adhesional origins from the dielectric standpoint (Reference 9). For this reason studies of similar surfaces must be included for complete understanding of the adhesive phenomenon. Cohesion present during adhesion studies becomes important for both theoretical understanding and for understanding of bulk effects on either side of interfaces. Cohesive forces contribute then not only to modulus and to the strength of materials but also to their adhesive properties by effects during surface contact through both reversible and irreversible deformations. Contributions of the dispersive forces to the mechanical properties have been mentioned previously (References 9 through 15).

The models of Harrison and others used bond rupture and formation to describe the adhesive hysteresis of a diamond-diamond surface, in which the interaction of a tip and substrate during a surface force experiment was simulated (References 50, 51, and 71). Interestingly, several mechanisms appear which may be directly related to the energy loss differentials needed for adhesion. First of all plastic deformation appeared to accompany an adhesive hysteretic interaction, but was not necessary. In lieu of deformation, bond formation also led to adhesion. Both mechanisms originated from specific orientations of the tip and substrate surface, guided by their specific potentials. For instance depending upon the surface state of the substrate (either hydrogen terminated or nonhydrogen terminated), approach of the tip was accompanied by specific alignment of the tip atoms over bonds (if the surface was hydrogen terminated) or atoms (if the surface was nonhydrogen terminated). This ultimately led to hysteresis depending upon the mechanisms resulting from the mutual orientations upon compression. For the hydrogen terminated surface, hysteresis appeared to originate from bond rupture or damage of the crystalline structure and subsequent bond formation upon high enough compression. For the nonhydrogen terminated surface, an adhesive "bond" was formed between hydrogen and the surface carbon radical, but did not involve the compression induced deformation mechanism; however bond rupture did occur upon unloading. This mechanism also occurred at lower compressive loads for the nonhydrogen terminated case than the hydrogen terminated case, leading to adhesion at earlier compressive loads. In both cases, the adhesive energy was thought to be derived through fracture mechanisms.

The dielectric models used previously to describe the adhesion of interacting surfaces does not necessarily require covalent bond rupture and formation to accompany adhesion. Polymer modeling is especially important when determining adhesive abilities because of the large industry devoted to polymer-based adhesives and composites. For these reasons, studies in polymers which include both bond potential and dispersive contributions have been made in order to direct predictions of modulus and strength trends (References 50, and 52 through 55). These studies were done using commercially available software (Discover 2.7 from Biosym Technologies, Inc., San Diego, Calif.) to

demonstrate the usefulness of Newtonian force field calculations on the prediction of modulus and strength. The mechanisms studied considered only the cohesive contributions of the polymers due to the dielectric mechanisms present and the energy losses upon dynamics because of internal bond deformations and mutual orientations. The simulations studied agreed with basic structural biases, which experimentally showed increased modulus with increased chain orientation to the force applied. In this way, rudimentary implications could be drawn on the effect of mutual orientation populations on the modulus of the bulk polymer.

The dynamics began with a minimized system, consisting of two mutually oriented chains (for example, see Figure 3). The assumption was made that modulus trends would primarily arise from the population of maximum chain to chain interactions, such as in an oriented chain and the distribution of force vectors on this interaction. For each case, the dynamics were set up in order to force the chains past one another at room temperature along their co-axis, simulating an uniaxial force. This was done by inducing acceleration on only two atoms defined one each on opposite ends of the two chains. It was reasoned that in this way all other effects (such as bond rotation, angle movement, and atom or group translation) were induced by the defined potentials or dielectric nature of the chains. Therefore, because of the nature of the simulation, the bond deformations (rotation, vibration, and translation) originated from not only the kinetic energy of temperature and deformation but from the cohesive nature of the Van der Waals and coulombic potentials, instead of concentrating on just rotational barriers of specific bonds. A perpendicular stress direction was also defined and compared in which the force was defined on one atom of each chain in the center of the chain which represented a second major force orientation.

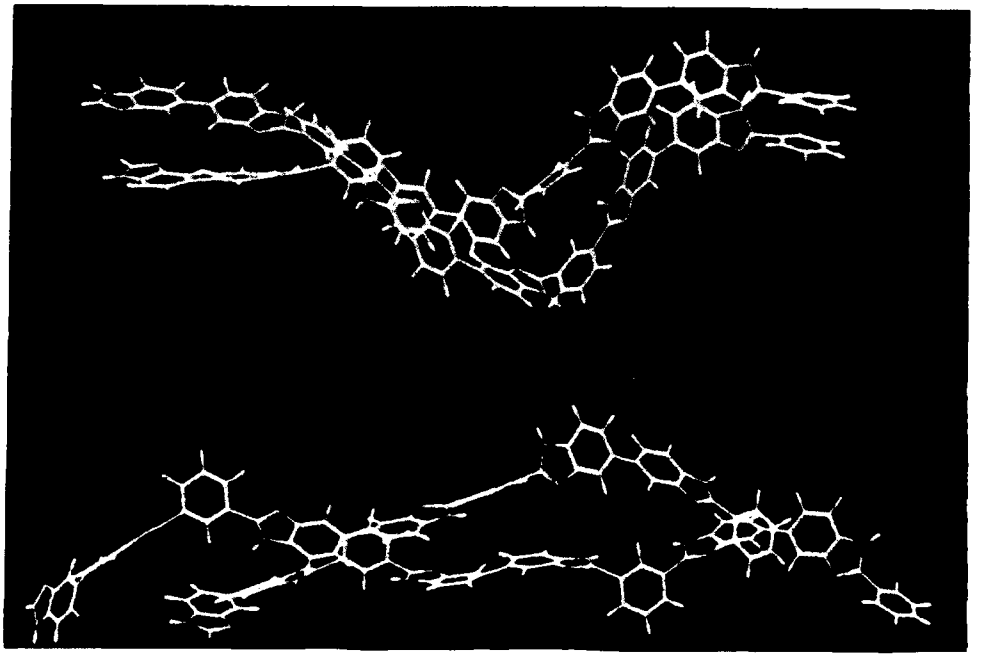

FIGURE 3. (a) Oriented Polybenzimidazole Model Before Stress Dynamics and (b) Polybenzimidazole After Uniaxial Stress Dynamics Defined Along Co-Axis.

The total energy diagrams obtained for studies of hydration effects on polybenzimidazole (PBI) were used to establish a trend of both modulus and strength predictions. These predictions were quantitative against the experimental moduli trends, and qualitative against the experimental strain-to-break and ultimate strength trends (References 52 and 53). The total energy diagrams obtained to trend moduli data for epon-828 agreed qualitatively with experimental data (Reference 55). For both systems, the models showed structurally dependent stress direction preferences (axial versus perpendicular) suggesting ways in which to predict orientation populations or to predict process preferences for attaining enhanced properties. In addition, the specific trajectories of the hydrated forms of polybenzimidazole began to show signs of chaotic behavior. It was theorized that the degradation of mechanical cohesiveness could originate from such pathways (Reference 54).

Finally, hysteresis curves were obtained for oriented polybenzimidazole (unhydrated) dynamic trajectories, where the uniaxial strain was taken from approximately 1.1 to 3.7% (the loading curves) and the chains allowed to relax without external forces (unloading or relaxation curves) (shown in Figures 4 through 9). The curves were obtained using the previous uniaxial stress trajectories (References 52 and 53), but the deformation process was interrupted at differing times from the beginning of the trajectory. The forcing potential was then eliminated, and the unconstrained dynamics were allowed to continue at room temperature for 0.5 to 1.0 picoseconds (ps) which served to relax the molecules from their higher energy strained configurations. In each case, the distance between the two forced atoms (which were originally used to pull the chains apart), were monitored to follow relaxation behavior upon removal of the constraining force.

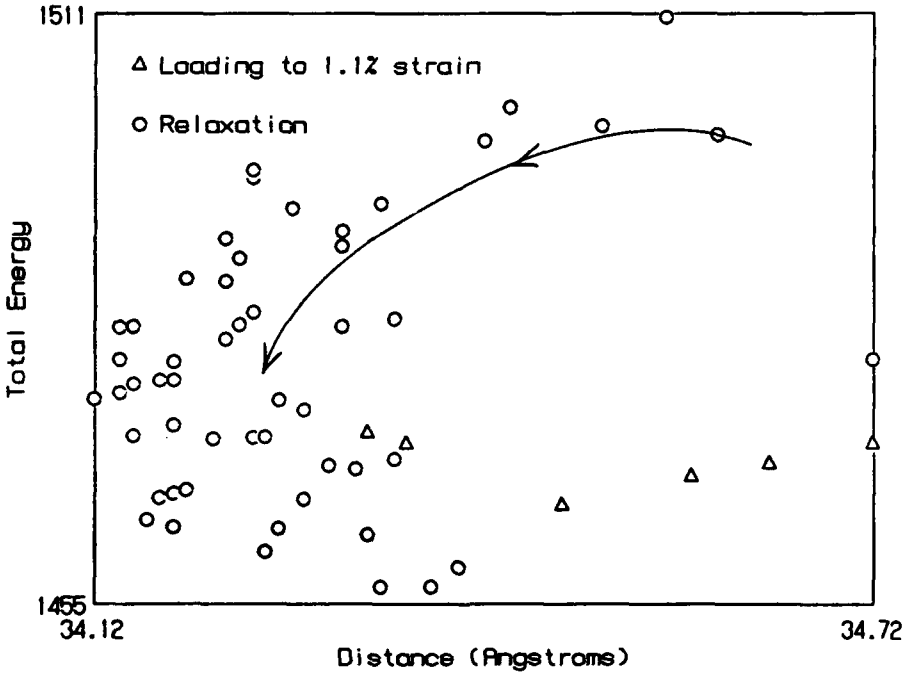

FIGURE 4. Hysteresis Curve of Polybenzimidazole Showing Stress Trajectory to 1.1% Strain (triangles) and Relaxation Trajectory (circles). Arrow indicates general trajectory pathway upon relaxation, showing high energy pathway to compressive state.

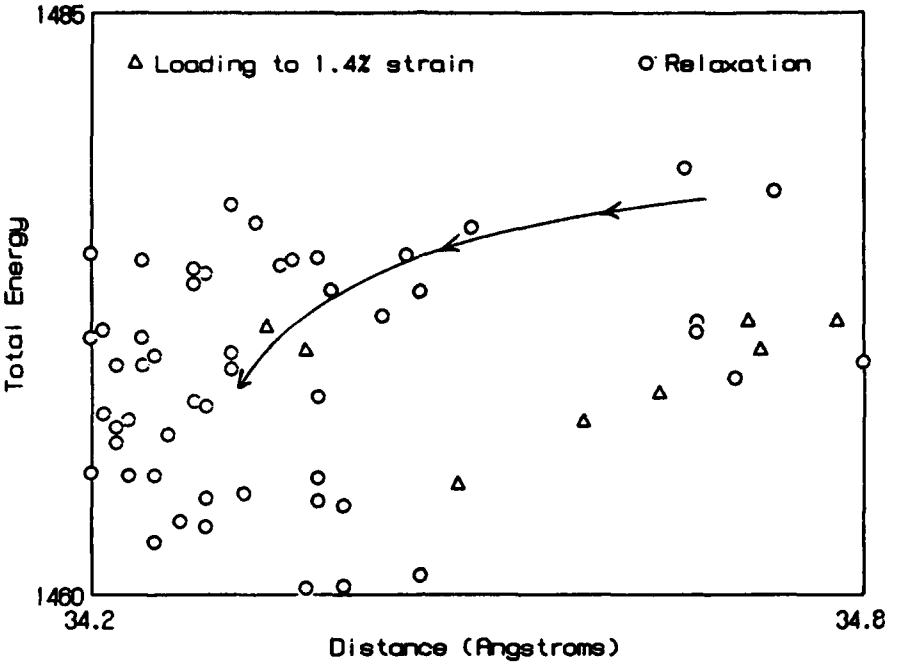

FIGURE 5. Hysteresis Curve of Polybenzimidazole Showing Stress Trajectory to 1.4% Strain (triangles) and Relaxation Trajectory (circles). Arrow indicates general trajectory pathway upon relaxation showing high energy pathway to compressive state.

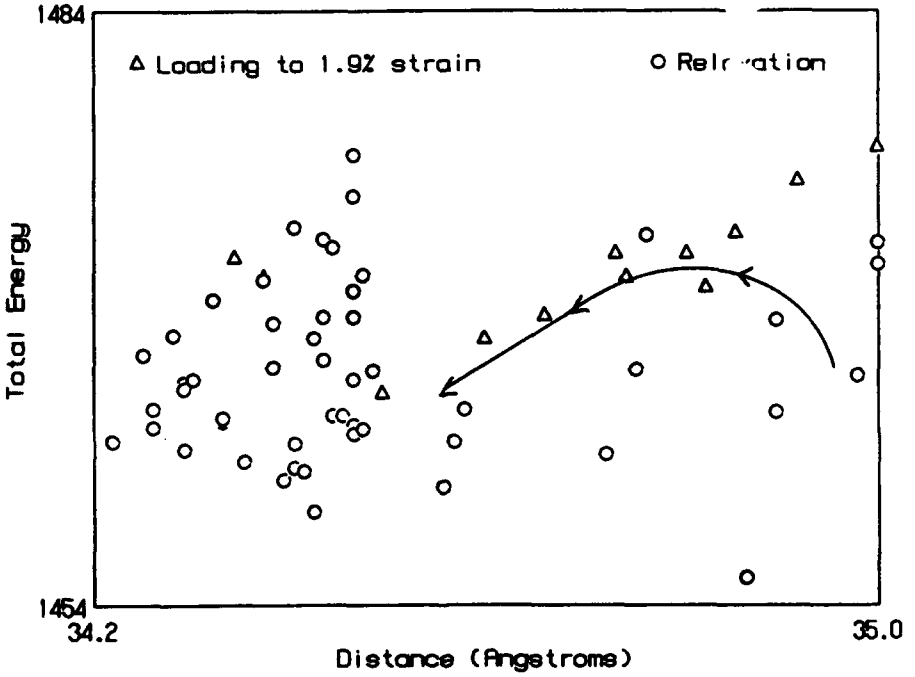

FIGURE 6. Hysteresis Curve of Polybenzimidazole Showing Stress Trajectory to 1.9% Strain (triangles) and Relaxation Trajectory (circles). Arrow indicates general trajectory pathway upon relaxation, showing the beginning of an alternate energy pathway.

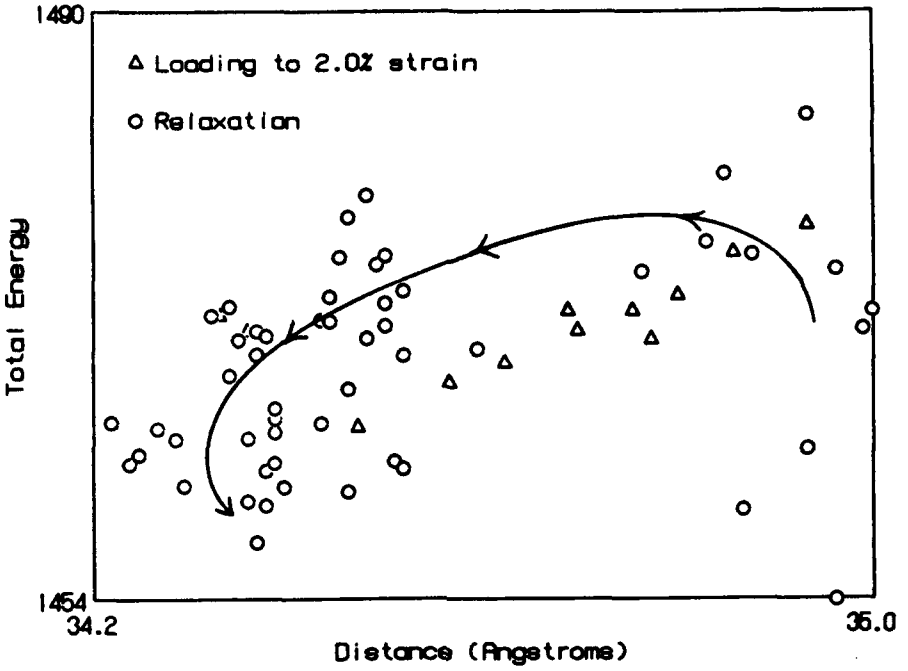

FIGURE 7. Hysteresis Curve of Polybenzimidazole Showing Stress Trajectory to 2.0% Strain (triangles) and Relaxation Trajectory (circles). Arrow indicates general trajectory pathway upon relaxation.

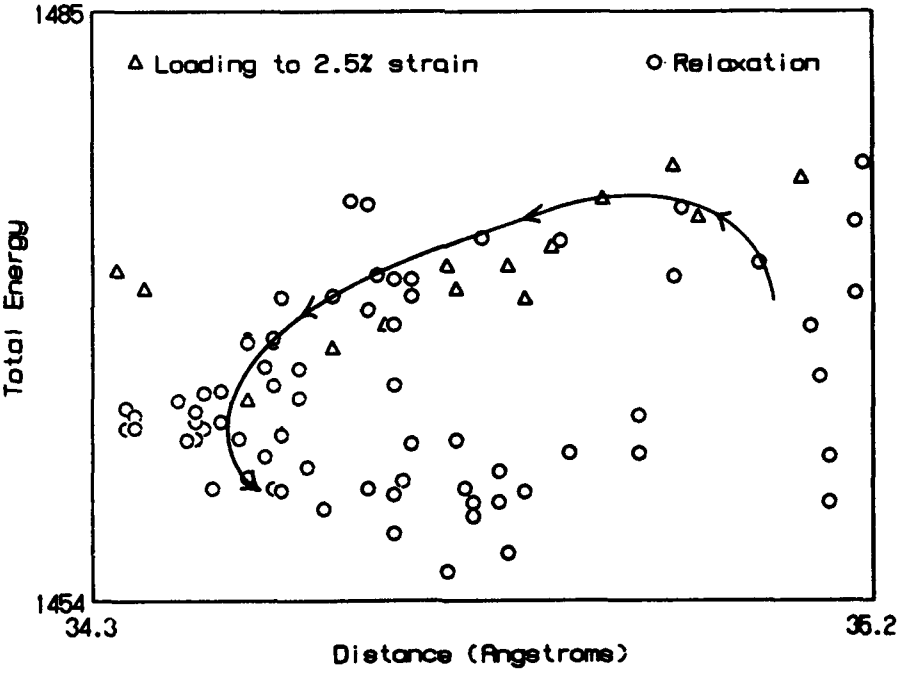

FIGURE 8. Hysteresis Curve of Polybenzimidazole Showing Stress Trajectory to 2.5% Strain (triangles) and Relaxation Trajectory (circles). Arrow indicates general trajectory pathway upon relaxation.

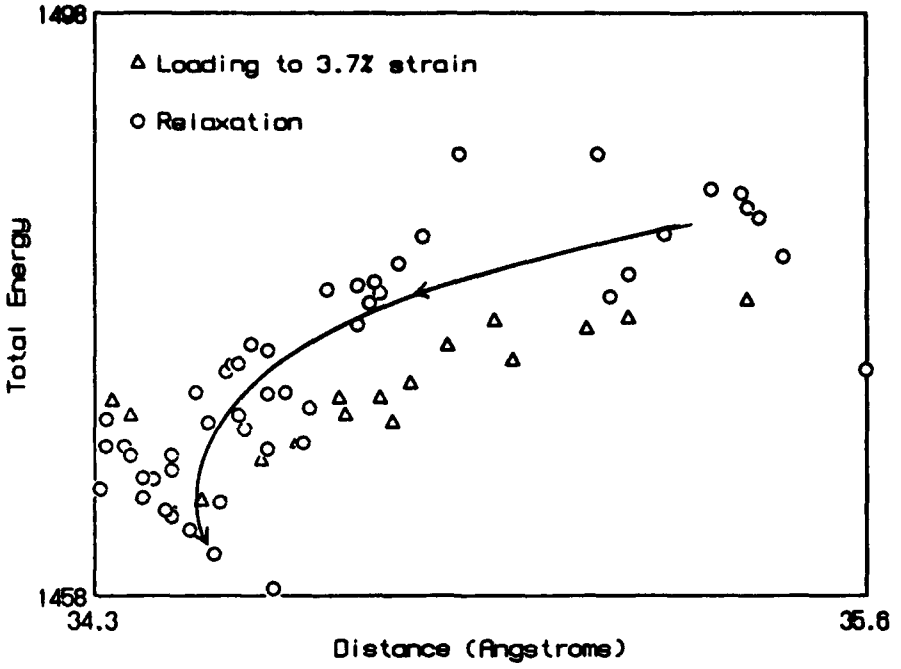

FIGURE 9. Hysteresis Curve of Polybenzimidazole Showing Stress Trajectory to 3.7% Strain (triangles) and Relaxation Trajectory (circles). Arrow indicates general relaxation pathway, showing energy reversibility into compression.

In each case, the relaxation trajectories exhibited a compressive state, relaxing to a final equilibrium state of lower energy and higher elongation than the original structure. This may be indicative of an accompanying stress-relaxation or creep mechanism. The development of an energetically reversible mechanism appeared by following the changing relaxation trajectories from the 1.1% (0.05 ps) case to the 3.7% (0.16 ps) strain case. Within the 1.1 (0.05 ps) to 1.4% (0.08 ps) strain range (Figures 4 and 5), the relaxation appeared to follow a higher energy pathway with decreasing (relaxing) strain which allowed the chains to first go into a high energy compression followed by energy relaxation into a low energy compressive state and equilibration close to the original strain but slightly elongated with respect to original structure and lower in energy. From the 1.9% (0.11 ps) strain in loading to approximately 2.5% (0.14 ps) strain (Figures 6 through 8), the relaxation pathway appeared to mechanistically change following a double cycle in which the energy immediately decreased with the decreasing strain, then increased in order to almost follow the reverse of the loading trajectory. However, the molecules deviated by going into compression near the energy minimum with the final equilibrium coalescing at a slightly lower energy and higher strain than the original structure. Because of the hysteresis, the relaxing chains never followed an exact reversible pathway. At the largest strain used (3.7%), the relaxation curve again appeared to change mechanistically following a similar shape as the lower strain relaxation with a slightly higher energy reverse pathway into slight compression. The closest reversible pathway to the loading curve was found during relaxation of the 3.7% strain (Figure 9) in which the loading and unloading (relaxation) curve were almost the same. However, at the end of the relaxation the molecules again followed a compressive pathway and began to reach equilibrium at a strain slightly larger than the original structure, again lower in energy. In all cases, the end

structure remained lower in energy and elongated in comparison to the original structure showing a hysteresis originating in bond rotation and slight chain translation, when compared with the original structure.

The polybenzimidazole curves cannot be directly compared with the diamond hysteresis curves of Harrison and others because of the different force fields and assumptions used (References 50, 51, and 71). For instance, the diamond force fields did not include contributions from rotational bonding and dispersional forces and did not include corrections for partial bonding or lone pair behavior. In addition, the diamond curves attempted to study the affects of two approaching surfaces. During the polybenzimidazole model, the surfaces (which are on a chain level) had already made contact and all dielectric components had been minimized in relationship to one another. The only PBI model remotely analogous to the approaching interface simulation of the diamond model could be considered the reverse trajectory of the large strain PBI model. In this case, deformations over 30% were used in order to force the pre-minimized chains apart past their initial barrier to deformation, again simulated at room temperature (References 52 and 53).

Because the PBI models were simulated from a smaller molecular scale instead of an expanded surface model scale, the convention of compression or tension cannot unequivocally be defined. Therefore, disregarding the above concerns, for the hysteresis curves, the uniaxial strain (or loading) on the two-chain polybenzimidazole system could be considered mechanically analogous with the compressive state of the diamond model, as generally both models brought the surfaces past minimum energies. The relaxation component of the polybenzimidazole hysteresis curve could then be compared to the unloading portion of the diamond model. However, the polybenzimidizole models, having started from the minimized structures, suggested that the initial cohesion (or attraction) was totally due to the dispersive and coulombic interactions, instead of bond formation as suggested in the diamond model. The hysteresis curves also indicated that energy loss of the polybenzimidazole systems was due to changes in both the conformational energy of the chains (as positions were rearranged slightly even at low deformations) and also due to the re-adjusted dispersive and coulombic energies. This is apparent in the relaxed structure which attained a lower energy with a higher strain than the starting structure. This is analogous to the atomic force data in which a lower energy (or a higher adhesive or attractive force) was achieved after compression of the interface. In an analogous adhesive bond, this may be interpreted as a deformation induced energy stabilization at the interface; however, what is unknown at this point is the change in the energy barrier to deformation of this newly interacting system.

CONCLUSION

This analysis has attempted to view the adhesion phenomenon in terms of dielectric components, in order to propose a way to view or categorize adhesion data for direct correlation to molecular properties. It is hoped that use of such dielectric trend analysis will help to isolate adhesion mechanisms which will lead to improved adhesive molecular structures. Both interface examples examined showed a strong correlation of adhesion to

the molecular dipole moments (permanent, induced, and instantaneous). Because of this, measurable quantities such as the static and high field dielectric constants may become simple indices for adhesion tendencies. For metal-dielectric interfaces, where the dielectric constant of the metal becomes meaningless, it was suggested that both the conductivity of the metal and the dielectric constant of the dielectric may serve as indices. But in general the adhesion mechanisms may become classified in terms of electric field interactions, field containment mechanisms, or any other mechanisms which encourage electronic work. However, the other case of metal-metal interfaces has not been addressed. It was also argued that because surface structure, geometry or topography played a large role in adhesion by its contribution to the defined surface reaction field, average properties such as the dielectric constant or molecular dipole moment would never show quantitative correlations. In addition, such indices were further complicated by the effects of plastic deformation on the total description of the adhesive bond. Deformation will affect adhesion by redefining the interface reaction field due to reorientations of the component dipoles, as well as redefining the extent of integration of the dipole moments for total interaction.

The role of surface structure may become clearer as better atomic force measurements of surface structures are made. For instance, because atomic force microscopy is able to sample surface dielectric properties, the surface fields may be quantitatively determined with respect to surface topography. And since the effects of molecular structure may be directly determined, computer simulations may be finally verified from the atomistic level. However the common denominator in all of the mechanisms, is the determination of the interaction fields which contribute to the energy loss mechanisms; from a dynamic standpoint this may be challenging to categorically define.

REFERENCES

1. K. D. Rendulic. "Sticking and Desorption: A Review," *Surface Sci.*, Vol. 272 (1992), pp. 34-44.

2. Jacob Israelachvili. "Interfacial Forces," *J. Vac. Sci. Technol. A.*, Vol. 10(5) (1992), pp. 2961-71.

3. C. Boiziau and G. Lecayon. "Adhesion of Polymers to Metals: a Review of the Results Obtained Studying a Model System," *Surface and Interface Analysis*, Vol. 12 (1988), pp. 475-485.

4. J. F. Watts. "The Application of Surface Analysis to Studies of the Environmental Degradation of Polymer to Metal Adhesion," *Surface and Interface Analysis*, Vol. 12 (1988), pp. 497-503.

5. J. J. Bikerman. *Physical Surfaces*, New York, Academic Press, 1970. 476 pp.

6. Milton J. Rosen. *Surfactants and Interfacial Phenomena*, New York, John Wiley & Sons, 1978. 304 pp.

7. Fred J. Meyer. "Adhesion and Bonding," in *Encyclopedia of Polymer Science and Engineering*, Vol. 1, ed. by Jacqueline I. Kroschwitz. New York, John Wiley & Sons. Pp. 478-546.

8. N. Gane, P. F. Pfaelzer, and D. Tabor. "Adhesion Between Clean Surfaces at Light Loads," *Proc. Royal Soc. London*, A 340 (1974), pp. 495-517.

9. J. N. Israelachvili and D. Tabor. "The Measurement of van der Waals Dispersion Forces in the Range 1.5 to 130 nm," *Proc. Royal Soc. London*, A 331 (1972), p. 19-38.

10. J. N. Israelachvili. "The Calculation of van der Waals Dispersion Forces Between Macroscopic Bodies," *Proc. Royal Soc. London*, A 331 (1972), pp. 39-55.

11. D. Tabor and R. H. S. Witherton. "The Direct Measurement of Normal and Retarded van der Waals Forces," *Proc. Royal Soc. London*, A 312 (1969), pp. 435-50.

12. Roger G. Horn and Jacob N. Israelachvili. "Direct Measurement of Structural Forces Between Two Surfaces in a Nonpolar Liquid," *J. Chem. Phys.*, 73(3) (1981), pp. 1400-11.

13. Jacob N. Israelachvili. "Adhesion Forces Between Surfaces in Liquids and Condensable Vapours," *Surface Sci. Reports*, 14 (1992), pp. 109-59.

14. David L. Allara and Ralph G. Nuzzo. "Spontaneously Organized Molecular Assemblies. 1. Formation, Dynamics and Physical Properties of n-Alkanoic Acids Adsorbed From Solution on an Oxidized Aluminum Surface," *Langmuir*, 1 (1985), pp. 45-52.

15. David L. Allara and Ralph G. Nuzzo. "Spontaneously Organized Molecular Assemblies. 2. Quantitative Infrared Spectroscopic Determination of Equilibrium Structures of Solution Adsorbed n-Alkanoic Acids on and Oxidized Aluminum Surface," *Langmuir*, 1 (1985), pp. 52-66.

16. Yves Martin, David W. Abraham, and H. Kumar Wickramasinghe. "High Resolution Capacitance Measurement and Potentiometry by Force Microscopy," *Appl. Phys. Lett.*, 52 (13) (1988), pp. 1103-05.

17. M. Nonenmacher, M. P. O'Boyle, and H. K. Wickramasinghe. "Kelvin Probe Microscopy," *Appl. Phys. Lett.*, 58 (25) (1991), pp. 2921-23.

18. E. Meyer, H. Heinzelmann, P. Grutter, Th. Jung, H. R. Hidber, H. Rudin, and J. Guntherodt. "Atomic Force Microscopy for the Study of Tribology and Adhesion," *Thin Solid Films*, 181 (1989), pp. 527-44.

19. Nancy A. Burnham and Richard J. Colton. "Measuring the Nanomechanical Properties and Surface Forces of Materials Using an Atomic Force Microscope," *J. Vac. Sci. Technol.*, A 7(4) (1989), pp. 2906-13.

20. Nancy A. Burnham, Dawn E. Dominguez, Robert L. Mowery, and Richard J. Colton. "Probing the Surface Forces of Monolayer Films with an Atomic Force Microscope," *Phys. Rev. Lett.*, 64(16) (1990), pp. 1931-34.

21. Nancy A. Burnham and Richard J. Colton. "Interpretation Issues in Force Microscopy," *J. Vac. Sci. Technol.*, A 9(4) (1991), pp. 2548-56.

22. Uzi Landman, W. D. Luedtke, Nancy A. Burnham, and Richard J. Colton. "Atomistic Mechanisms and Dynamics of Adhesion, Nanoindentation and Fracture," *Science*, 248 (1990), pp. 454-61.

23. Steven M. Hues, Richard J. Colton, Ernst Meyer, and Hans-Joachim Guntherodt. "Scanning Probe Microscopy of Thin Films," *MRS Bulletin*, January 1993, pp. 41-49.

24. N. A. Burnham, R. J. Colton, and H. M. Pollock. "Work-Function Anisotropies as an Origin of Long-Range Surface Forces," *Phys. Rev. Lett.*, 69(1) (1992), pp. 144-47.

25. C. J. F. Bottcher. *Theory of Electric Polarization*, Amsterdam, Elsevier Scientific Publishing Co., 1973. 377 pp.

26. A. D. McLachlan. "Effect of the Medium on Dispersion Forces in Liquids," *Discussions of the Faraday Soc.*, Vol. 40 (1965), pp. 239-45.

27. A. D. McLachlan. "Retarded Dispersion Forces in Dielectrics at Finite Temperatures," *Proc. Royal Soc. London*, Series A 274 (1963), pp. 80-90.

28. A. D. McLachlan. "Retarded Dispersion Forces Between Molecules," *Proc. Royal Soc. London*, Series A 271 (1963), pp. 387-401.

29. S. S. Voyutskii. *Autoadhesion and Adhesion of High Polymers*, London and Sydney, Interscience Publ., 1963.

30. Antonio Redondo, Yehuda Zeiri, and William A. Goddard III. "Application of Transition State Theory to Desorption from Solid Surfaces: Ammonia on Ni (111)," *J. Chem. Phys.* 79(12) (1983), pp. 6410-15.

31. Antonio Redondo, Yehuda Zeiri, and William A. Goddard III. "Classical Stochastic Diffusion Theory for Desorption of Atoms and Molecules From Solid Surface," *Am. Phys. Soc.*, 49(25) (1982), pp. 1847-50.

32. Antonio Redondo, Yehuda Zeiri, and William A. Goddard III. "Classical Stochastic Diffusion Theory for Thermal Desorption From Solid Surfaces," *J. Vac. Sci. Technol. B*, 2(3) (1984), pp. 550-60.

33. K. L. Johnson, K. Kendall, and A. D. Roberts. "Surface Energy and the Contact of Elastic Solids," *Proc. Royal Soc. London*, A 324 (1971), pp. 301-13.

34. Barton Dahneke. "The Influence of Flattening on the Adhesion of Particles," *J. Colloid and Interface Sci.*, 40(1) (1972), p. 1-13.

35. J. F. Silvain, A. Veyrat, and J. J Ehrhardt. "Effect of Temperature on the Adhesion and the Morphology of Thin Metal Films Evaporated on Polyethylene Terephthalate," *Thin Solid Films*, 221 (1992), pp. 114-19.

36. R. Flitsch and D. Y. Shih. "A Study of Modified Polyimide Surfaces as Related to Adhesion," *J. Vac. Sci. Technol.*, A 8(3) (1990), pp. 2376-81.

37. F. J. Boerio, P. P. Hong, H. W. Tsai, and J. T. Young. "Non-destructive Characterization of Polymer/Metal Interfaces Using Surface-Enhanced Raman Scattering," *Surface and Interface Analysis*, Vol. 17 (1991), pp. 448-56.

38. Michael C. Burrell, G. M. Porta, B. R. Karas, D. F. Foust, and J. J. Chera. "Copper Deposition Onto Polyetherimide: Interface Composition and Adhesion," *J. Vac. Sci. Technol.*, A 10(4) (1992), pp. 2752-57.

39. Lj. Atanasoska, Steven G. Anderson, H. M. Meyer III, Zhangda Lin, and J. H. Weaver. "Aluminum/Polyimide Interface Formation: an X-Ray Photoelectron Spectroscopy Study of Selective Chemical Bonding," *J. Vac. Sci. Technol.*, A 5(6) (1987), pp. 3325-33.

40. J. Lynn Davis, Melanie Williams, J. Kevin Arledge, and Tom Swirbel. "Spectroscopic Studies of the Chemical Properties of Thin Metal Films on Poly(etherimide)," *Thin Solid Films*, 220 (1992), pp. 217-21.

41. I. Kondo, T. Yoneyama, K. Kondo, O. Takenaka, A. Kinbara. "Effects of Different Pretreatments on the Surface Structure of Silicon and the Adhesion of Metal Films," *J. Vac. Sci. Technol.*, A 10(5) (1992), pp. 3166-70.

42. J. Krim, E. T. Watts, and J. Digel. "Slippage of Simple Liquid Films Adsorbed on Silver and Gold Substrates," *J. Vac. Sci. Technol.*, A 8(4) (1990), pp. 3417-20.

43. Jian-Sheng Wang and Kurt Binder. "Chain Linear Dimensions in the Surface Enriched Layer of Polymer Mixtures," *Makromol. Chem, Theory Simul.*, 1 (1992), pp. 49-53.

44. Thomas D. Hahn and Jeffrey Kovac. "Computer Simulation of the Dynamics of a Polymer Chain Terminally Attached to a Rigid Flat Surface," *Macromolecules*, Vol. 23 (1990), pp. 5153-54.

45. Doros N. Theodorou. "Variable Density Model of Polymer Melt/Solid Interfaces: Structure, Adhesion Tension, and Surface Forces," *Macromolecules*, Vol. 22 (1989), pp. 4589-97.

46. Doros N. Theodorou. "Variable Density Model of Polymer Melt Surfaces: Structure and Surface Tension," *Macromolecules*, Vol. 22 (1989), pp. 4578-89.

47. Dwight E. Gray, coordinating ed. *American Institute of Physics Handbook, Third Edition*, New York, McGraw-Hill, 1972.

48. David R. Lide, ed. *CRC Handbook, 72nd Edition*, Boca Raton, CRC Press, 1991-92, pp. 12-33.

49. "Ti Oxide for Adhesion Layers May Enable Al Replacement with Au, Ag or Cu," reported in *Semiconductor International*, June 1993, p. 17.

50. J. A. Harrison, D. W. Brenner, C. T. White, and R. J. Colton. "Atomistic Mechanisms of Adhesion and Compression of Diamond Surfaces," *Thin Solid Films*, 206 (1991), pp. 213-19.

51. J. A. Harrison, C. T. White, R. J. Colton, and D. W. Brenner. "Nanoscale Investigation of Indentation, Adhesion and Fracture of Diamond (111) Surface," *Surface Sci.*, 271 (1992), pp. 57-67.

52. Naval Air Warfare Center Weapons Center. *Molecular Modeling Study on the Mechanical Properties of Polybenzimidazole*, by N. Iwamoto. China Lake, Calif., NAWCWPNS, July 1992. 34 pp. (NAWCWPNS TP 8036, publication UNCLASSIFIED.)

53. N. Iwamoto. "A Property Trend Study of Polybenzimidazole Using Molecular Modeling," *Polym. Eng. and Sci.* (accepted for publication).

54. N. Iwamoto. "Molecular Dynamics of Polybenzimidazole and Contributions from Chaos," *Polym. Eng. and Sci.* (accepted for publication).

55. N. E. Iwamoto. "Epoxy-Curative Comparisons Using Dynamic Molecular Modeling" (publication in progress).

56. David Proter. "Viscosity as a Consequence of Dielectric Dissipation: 3. Complex Modulus Through Intermolecular Forces," *Polymer*, Vol. 28 (1987), pp. 1652-1656.

57. R. Elwell, D. Hayward, and R. A. Pethrick. "Delayed Action Pressure-Sensitive Adhesives: Correlation of Dielectric and Mechanical Properties," *Int. J. Adhesion and Adhesives*, Vol. 13 (1993), pp. 9-14.

58. G. N. Ingo, G. Scavia, and L. Giorgi. "Effect on Lacquer Adhesion of Solid State Properties of Tin Oxides," *Thin Solid Films*, Vol. 228 (1993), pp. 218-221.

59. D. E. Packham, P. J. Hine, and E. El Muddarris. "Epoxy Resins and Metals with Microfibrous Surface Topography," in *Adhesion 10*, ed. by K. W. Allen. London and New York, Elsevier Applied Sciences Publ., 1986, pp. 81-95.

60. J. R. G. Evans and D. E. Packham. "Adhesion of Polyethylene to Copper: Importance of Substrate Topography," *J. Adhesion*, Vol. 10 (1979), pp. 39-47.

61. J. R. G. Evans and D. E. Packham. "Adhesion of Polyethylene to Metals: The Role of Surface Topography," *J. Adhesion*, Vol. 10 (1979), pp. 177-91.

62. Motowo Takayanagi. "Crystallized State of Polymer in its Dispersion Behaviour," *Pure and Appl. Chem.*, Vol. 15 (1967), pp. 555-86.

63. Walter H. Stockmayer. "Dielectric Dispersion in Solutions of Flexible Polymer," *Pure and Appl. Chem.*, Vol. 15 (1967), pp. 539-54.

64. A. M. North. "Dielectric Relaxation in Polymer Solutions," *Chemical Society Reviews*, Vol. 1 (1972), pp. 49-72.

65. A. M. North. "Relaxation Studies of Environmental Effects in Solid Polymers," *Pure and Appl. Chem.*, Vol. 39 (1974), pp. 265-74.

66. Uzi Landman, W. D. Luedtke, and M. W. Ribarsky. "Structural and Dynamical Consequences of Interactions in Interfacial Systems," *J. Vac. Sci. Technol.*, A 7(4) (1989), pp. 2829-39.

67. Uzi Landman, R. N. Barnett, D. L. Cleveland, and R. H. Rast. "Theoretical Considerations of Energetics, Dynamics and Structure at Interfaces," *J. Vac. Sci. Technol.*, A 3(3) (1985), pp. 1574-87.

68. Donald W. Brenner. "Empirical Potential for Hydrocarbons for use in Simulating the Chemical Vapor Deposition of Diamond Films," *Phys. Rev. B.*, 42(15) (1990), pp. 9458-70.

69. G. C. Abell. "Empirical Chemical Pseudopotential Theory of Molecular and Metallic Bonding," *Phys Rev B.*, 31(10) (1985), pp. 6184-96.

70. D. W. Brenner, J. A. Harrison, C. T. White, and R. J. Colton. "Molecular Dynamics Simulations of the Nanometer-Scale Mechanical Properties of Compressed Buchminsterfullerence," *Thin Solid Films*, Vol. 206 (1991), pp. 220-23.

71. J. A. Harrison, C. T. White, R. J. Colton, and D. W. Brenner. "Molecular Dynamic Simulations of Atomic Scale Friction of Diamond Surfaces," *Phys. Rev. B.*, 46 (15) (1992), pp. 9700-8.

INITIAL DISTRIBUTION

1 Army Research Development and Engineering Center, Natick (SATNC-YSM, J. Walker)
2 Defense Technical Information Center, Alexandria